

Topographic Maps of Visual Space in the Human Cerebellum

Highlights

- The cerebellum contains multiple retinotopic maps of visual space
- Retinotopic visual selectivity is found in 3 clusters, located in OMV, VIIb, and VIIIb
- These topographic maps represent visual space similarly to the cerebral visual system
- We provide an atlas of retinotopic regions in the human cerebellum

Authors

Daniel M. van Es,
Wietske van der Zwaag,
Tomas Knapen

Correspondence

tknapen@gmail.com

In Brief

van Es et al. find the cerebellum's responses to visual stimuli to be retinotopically organized and highly similar to visual responses in the cerebral visual system. They publish an atlas of 5 visually selective regions in 3 cerebellar clusters.



Topographic Maps of Visual Space in the Human Cerebellum

Daniel M. van Es,¹ Wietske van der Zwaag,² and Tomas Knapen^{1,2,3,4,*}

¹Behavioral and Movement Sciences, Vrije Universiteit Amsterdam, Amsterdam 1081, the Netherlands

²Spinoza Centre for NeuroImaging, Royal Dutch Academy of Sciences, Amsterdam 1105, the Netherlands

³Twitter: @tknapen

⁴Lead Contact

*Correspondence: tknapen@gmail.com

<https://doi.org/10.1016/j.cub.2019.04.012>

SUMMARY

The purported role of the cerebellum has shifted from one that is exclusively sensorimotor related to one that encompasses a wide range of cognitive and associative functions [1–5]. Within sensorimotor areas of the cerebellum, functional organization is characterized by ipsilateral representations of the body [6]. Yet, in the remaining cerebellar cognitive and associative networks, functional organization remains less well understood. Regions of cerebral cortex [7–9] and subcortex [10] important for visual perception and cognition are organized topographically: neural organization mirrors the retina. Recently, it was shown that known retinotopic areas in cerebral cortex are functionally connected to nodes in the cerebellum [2, 11, 12]. In fact, this revealed signals with visuospatial selectivity in the cerebellum [13]. Here, we analyzed the highly powered Human Connectome Project (HCP) retinotopy dataset [14] to create a comprehensive and detailed overview of visuospatial organization in the cerebellum. This revealed 5 ipsilateral topographic maps in 3 cerebellar clusters (oculomotor vermis [OMV]-lobule VIIb-lobule VIIIb), of which we quantified visual field coverage and topography. These quantifications dovetail with the known roles of these areas in eye movements (OMV) [5, 15], attention (OMV-VIIb) [5, 13], working memory (VIIb) [13], and the integration of visuomotor information with respect to effector movements (VIIIb) [5]. To aid future research on visual perception in the cerebellum, we provide an online atlas of the visuospatial maps in Montreal Neurological Institute (MNI) space. Our findings demonstrate that the cerebellum is abundant with visuospatial information and, moreover, that it is organized according to known retinotopic properties.

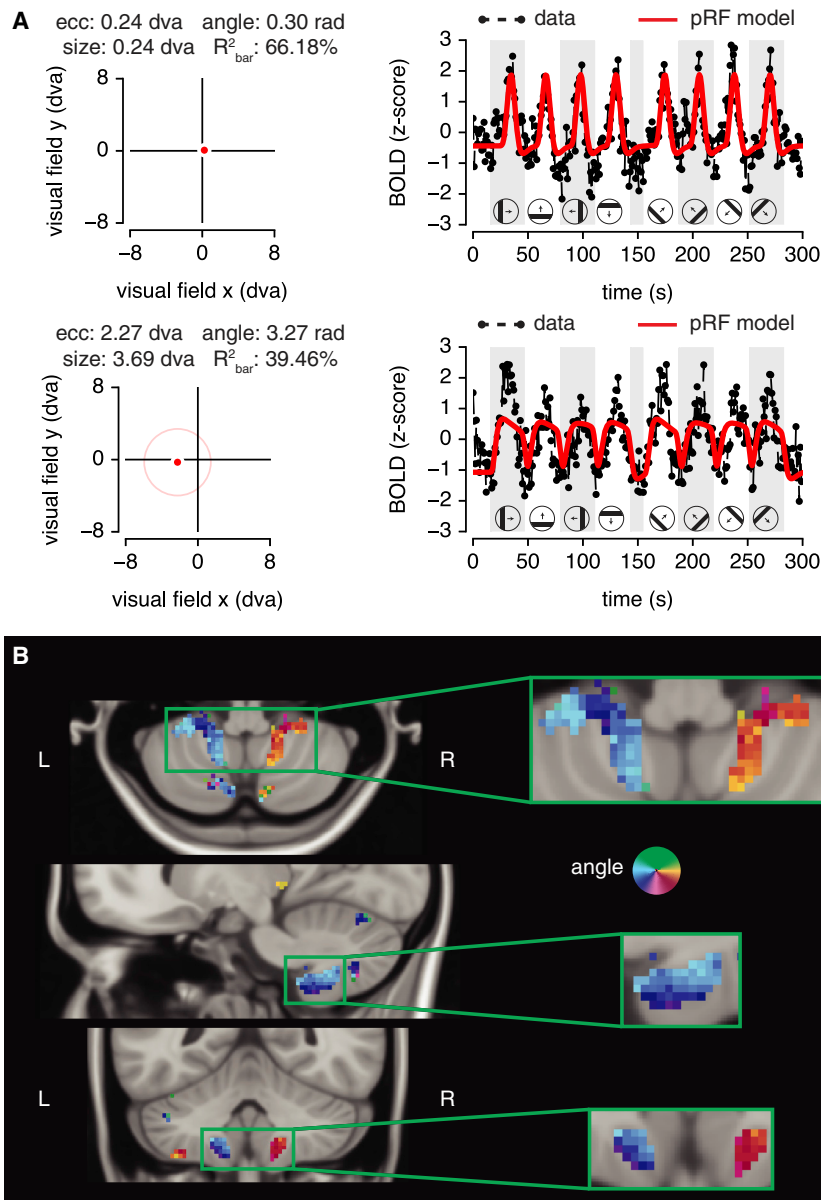
RESULTS AND DISCUSSION

The population receptive field (pRF) [16] model describes voxels' visual field response preferences with a concise set of spatial pa-

rameters. Specifically, the Human Connectome Project (HCP) retinotopy dataset [14] contains pRF parameters for the whole brain fitted on high-resolution 7T blood-oxygen-level-dependent (BOLD) responses to visual retinotopic stimulation during fixation. pRFs were fitted on data from individual participants ($n = 181$) and on an across-participant time course average (HCP "average participant"). As BOLD signal-to-noise ratio (SNR) is relatively low in the cerebellum [17], this dataset provides an unprecedented opportunity to characterize cerebellar retinotopic organization. Figure 1A shows two example pRFs with different sizes and eccentricities in the cerebellum, indicating cerebellar responses that are tightly coupled to visual-spatial stimulation. Visualizing pRF polar angle for each voxel in the volume reveals smooth progressions of pRF positions in the ipsilateral visual field (Figure 1B; see Figure S1 for an overview of all clusters in the volume). To better inspect the topographic structure of visual-spatial representations in the cerebellum, we projected pRF parameters for each cerebellar voxel onto a flattened representation of the cerebellum [18]. This revealed three clusters where the pRF model explained considerable variance (Figures 2A–2D; see Figure S2 for the voxel selection procedure and Figure S3 for results on both within- and across-participant consistency). We refer to the clusters as OMV (oculomotor vermis), VIIb, and VIIIb (see Figures 2G and 2H, top). The distribution of pRF centers within each of the clusters (Figure 2C) is characterized by representations of the ipsilateral visual field. This is opposite to the contralateral visual field representations in subcortical [10] and cortical [7] retinotopic areas. Yet it matches the ipsilaterality of the cerebellar somatotopic homunculi [6], resulting from midline crossing of cerebellar connective fibers in the pons [19]. Quantifications of the progressions of polar angle (Figure 2G) reveal a double representation of the lower visual field in OMV and VIIIb, separated by a phase reversal—as is common in cerebral visual cortex [7]. Finally, smooth variations in preferred eccentricity take place in the direction roughly orthogonal to the direction of polar angle phase reversals, again mirroring the organization of cerebral visual cortex (Figure 2H). Figures 2E and 2F provide a visual model summary of these retinotopic properties.

We next analyzed whether standard retinotopic properties (such as overrepresentation of the fovea and a strong correlation between pRF eccentricity and size) [7] were also present in the cerebellar polar angle and visual field maps (Figure 3). As Figure 2G revealed double representations of the visual field in OMV and VIIIb, we split these clusters into a medial and lateral



**Figure 1. Visual Responses in Cerebellum**

(A) Example compressive spatial summation (CSS) pRF profiles and fits for two voxels with different eccentricities and sizes. The dot in the visual field plot (left) indicates pRF center; the circle indicates pRF size at one SD. The example time course (right) is the average across the two bar-stimulus runs. Explained variance displayed here (R^2_{bar}) is calculated across the fits and time courses shown.

(B) pRF polar angle in the volume. Insets highlight a cluster with ipsilateral progressions of the visual field.

Also see Figures S1 and S4. Data in this figure are from the HCP “average participant.”

data from individual HCP participants were not sufficient to uncover all of these organizational principles (Figure S3A). However, the results are stable across split-halves of the entire dataset, both across participants and across runs (Figures S3B–S3E). Importantly, the polar angle reversals in OMV and VIIlb are consistent across the data splits (Figure S3E), indicating that the topographic structure of these areas is robust. To uncover whether the maps can be identified in single participants, we performed a separate high-powered retinotopic mapping experiment, also at 7T (see Figure S4). This indeed resulted in three cerebellar clusters that were well explained by the pRF model, matching the anatomical locations of OMV, VIIlb, and VIIIlb. In addition, these clusters preferred the ipsilateral visual field, and flattened angular progressions largely corresponded to those found in the HCP data. Together, this shows that the cerebellar visual field maps follow known properties of retinotopic organization, albeit with unique idiosyncrasies (i.e., ip-

portion separated by the line of polar angle reversal (Figure 3A). Visualizing the eccentricity distributions (Figure 3B) quantifies the observation described above: that eccentricity coverage is peri-foveal in OMV, extends somewhat into the periphery in VIIlb, and covers the full range of stimulated eccentricities in VIIIlb. Importantly, Figure 3C reveals clear increases in pRF size with increasing eccentricity in VIIlb and VIIIlb, with the range of eccentricities in OMV too small to ascertain this relation. Therefore, we refer to the OMV maps as polar angle maps instead of visual field maps. Finally, histograms of polar angle preference from left and right hemisphere separately (Figure 3D) highlight (1) the strong ipsilateral visual field representations and (2) a strong overrepresentation of the lower visual hemifield in VIIIlb. We verified the robustness of these characteristics by performing split-half analyses both across runs and across participants (see Figure S3). Specifically, this showed that the 30 min of retinotopic mapping

silaterality and strong overrepresentations of the fovea in OMV and of the lower visual field in OMVlat and VIIIlb. We note that a large amount of data (either many participants or many experimental runs) is required to uncover these principles. This can explain why topographic organization in the cerebellum has previously gone unnoticed (although see [13]). The required large amount of data could be due to the fact that SNR is generally lower in the cerebellum compared to the cortex [17]. However, new developments in the field of magnetic resonance (MR) are fast improving the cerebellar SNR [17]. In addition, it must be noted that these maps were studied using standard retinotopic mapping procedures that are optimized to evoke responses in the cortical visual system. Alternative experimental protocols tuned to the functional properties of the cerebellar clusters might additionally contribute to evoking larger responses, thus increasing the functional contrast to noise ratio.

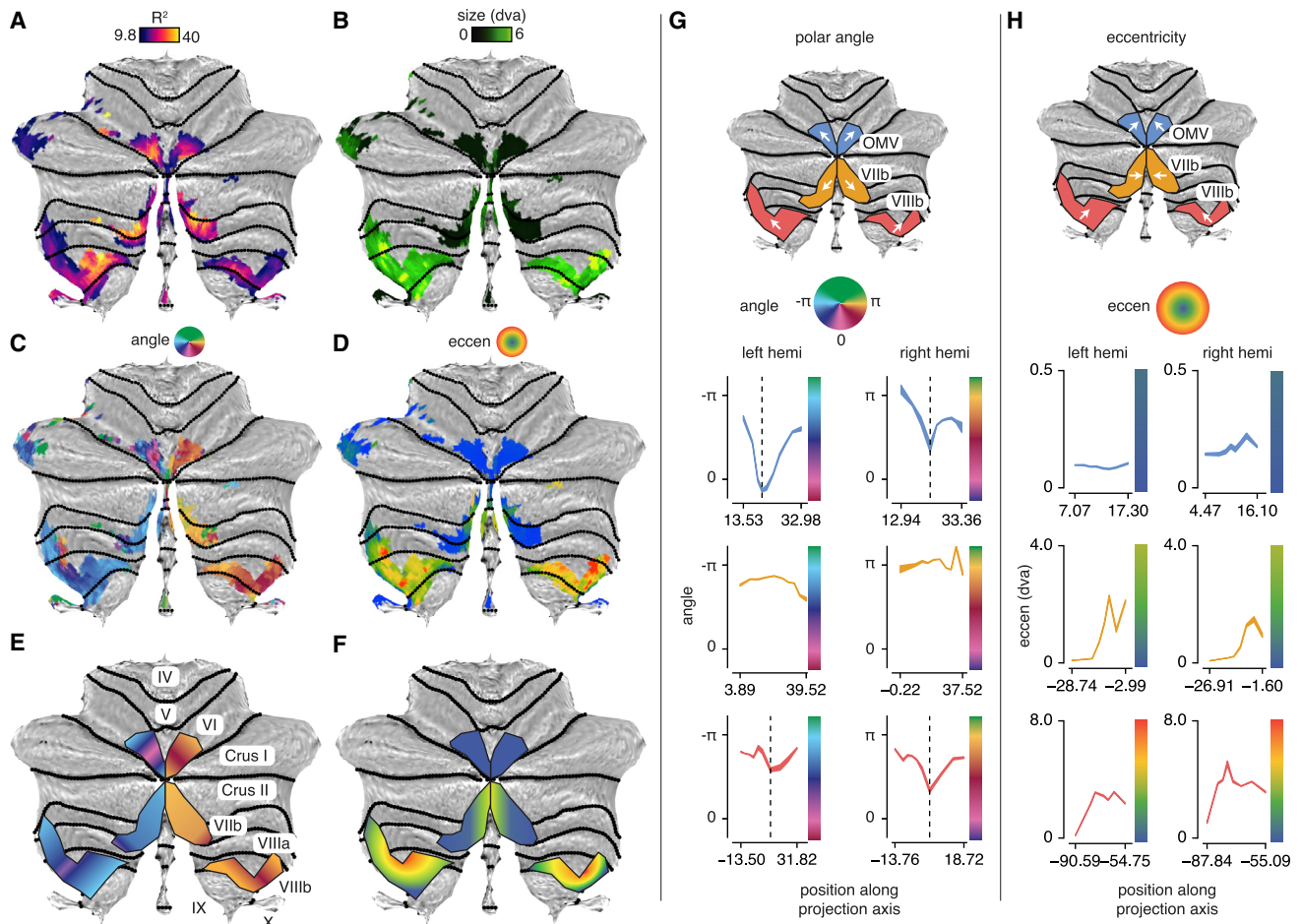


Figure 2. pRF Parameters Projected onto a Flattened Cerebellar Representation

(A–D) Flattened representation of pRF explained variance (A), size (B), polar angle (C), and eccentricity (D) reveals three retinotopic clusters in the cerebellum. (E and F) Summarized representation of pRF polar angle (E) and eccentricity (F). (G and H) pRF polar angle (G) and eccentricity (H) projected on a line in two-dimensional spatially unbiased atlas template (SUIT) of the cerebellum surface space. The direction of projection is indicated by the white arrows in the flat maps displayed above the data. Data line width in the lower panels reflects 95% confidence intervals of the mean across vertices in the average HCP participant for each decile in the projected vertices, and the units on the abscissa are millimeters on the cerebellar surface. This reveals double representations of the lower visual field in OMV and VIIIb (dashed vertical lines demarcate polar angle reversals). Data in this figure are from the HCP average participant. The full range of the color bars in (H) is [0,8] degrees of visual angle. See Figure S2 for the voxel selection procedure, see Figure S3 for split-half analyses of these data across runs and across participants and for results of individual HCP participants, and see Figure S4 for the newly collected individual participant data.

The OMV is implicated in the deployment of spatial attention and in the generation and adaptation of saccades [5, 15] (see Figure 4C). In accordance with the polar angle progressions we find, direction selectivity of OMV Purkinje cells has been shown to arise as a function of saccade error direction and is also organized along an anatomical gradient [20]. But OMV neurons encode saccade amplitude (and the corresponding visual eccentricity of the saccade target) by the duration of a population response rather than by tuning [21]. In correspondence, we do not find strong eccentricity tuning progressions in OMV. We consider these neuronal properties as possible explanations of the retinotopic properties of the OMV cluster, keeping in mind the caveat that the link between BOLD signals and spiking behavior differs between cerebellar and cerebral cortex [22].

The anatomical location and extent of VIIIb matches closely with a cerebellar component of the dorsal attention network [2, 11, 13] (see Figure 4A). Region VIIIb was recently shown to (1) be functionally connected with the intraparietal sulcus (IPS) and (2) to inherit visuospatial selectivity from these retinotopically organized cortical regions (see Figure S4E for a side-by-side comparison of that study to the present results [13]). Together, this suggests that VIIIb is mainly involved in spatial cognition, including attention and working-memory-related processes.

Cluster VIIIb overlaps with cerebellar components of both the dorsal and ventral attention networks and with the somatomotor network (see Figure 4A). In addition, data from the HCP project [3] showed that this region is activated by motor tasks (Figure 4B), especially by foot-related movements

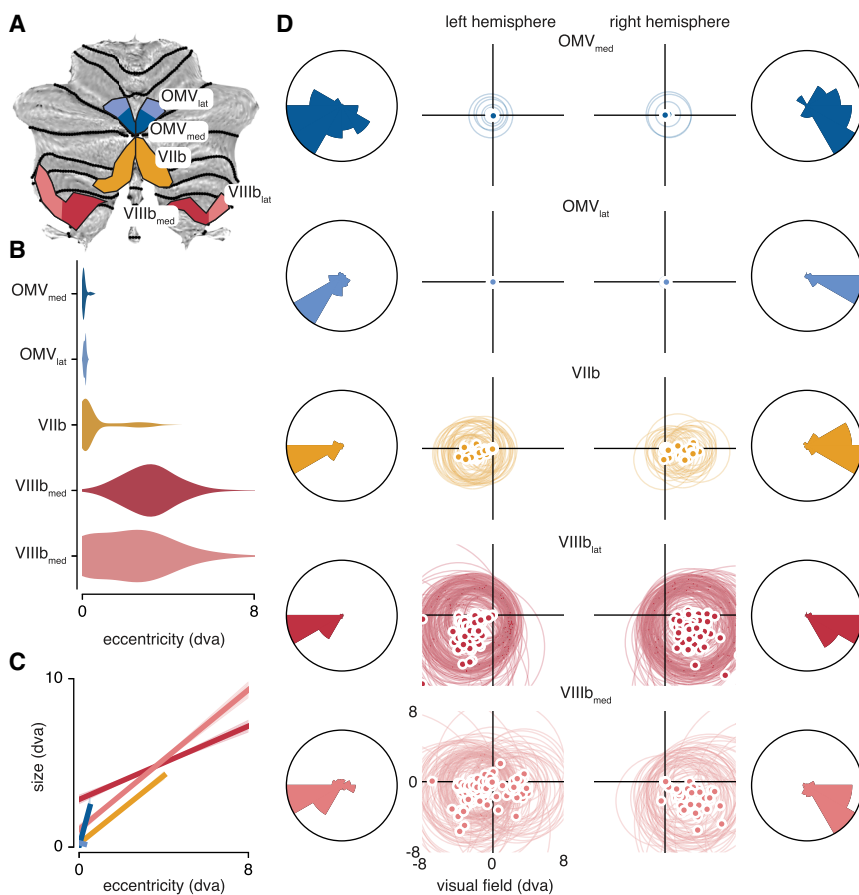


Figure 3. Distribution of pRF Properties within Cerebellar Visual Field Maps

(A) Region of interest (ROI) legend.

(B) Distribution of pRF eccentricities.

(C) pRF eccentricity versus size relations. Lines indicate linear regression fits with shaded regions representing 95% confidence intervals obtained by bootstrapping across voxels in the HCP average participant.

(D) Distribution of pRFs throughout the visual field. Dots indicate pRF centers; circles indicate pRF size (one SD). The polar histograms depict pRF center distributions. The histograms are normalized with respect to the maximum voxel count to highlight differential relative distributions across ROIs. This shows (1) strong ipsilaterality in all maps and (2) strong overrepresentations of the fovea in OMV and of the lower visual field in OMV_{lat} and VIIlb.

All data in this figure are from the HCP average participant. See Figure S3 for split-half analyses of these data across runs and across participants and for results of individual HCP participants. dva, degrees of visual angle.

(Figure 4D). This could suggest an integrative role for this region, binding together attentional and motor processes. Indeed, a recent functional parcellation of the cerebellum showed that cluster VIIlb is mainly related to “action observation” and to “hand presses” (Figure 4C). The action observation in that study reflected the observation of two hands tying different knots. Together, this suggests that this region may be involved in the integration of visuospatial information for the guidance of effector movements. In line with this idea, visual field coverage in VIIlb was strongly biased to the lower visual field, where behavioral performance is superior for stimuli associated with visuomotor coordination [23]. The strong foveal bias in OMV and the lower visual field preference in VIIlb show that, in addition to its strong similarities with cerebral visual processing, visual processing in the cerebellum is also idiosyncratic. More detailed mapping of the selectivities of these regions is needed to elucidate these idiosyncrasies.

We would like to note that retinotopic mapping under fixation precludes the distinction between purely retinotopic (eye-centered), craniotopic (head-centered), spatiotopic (world-centered), and other spatial encoding schemes. It is likely that cerebellum encodes visual information such that it can share this information with other effectors for action, and our findings can serve as a starting point for oculomotor research into the reference frames the cerebellum uses to encode spatial information.

The 7T pRF mapping experiment we performed highlights that cerebellar fMRI is strongly constrained by the fact that signal quality is generally low in the cerebellum. For instance, we find that visuospatial selectivities are less stable in area VIIlb, which is closest to the brainstem. This causes marked decreases in signal

quality in this region, possibly due to diminished transmit power and/or pulsation artifacts. We argue that future imaging advances aimed at improving cerebellar signal quality will be instrumental in opening up the cerebellum to increased scrutiny.

In sum, our results uncover 5 visuospatial maps in three topographically organized clusters in the cerebellum. This shows that visuospatial signals in the cerebellum are (1) much more abundant than was previously assumed [1–5] and (2) follow classical properties of retinotopic organization as identified in cortical [7] and subcortical [10] regions.

STAR★METHODS

Detailed methods are provided in the online version of this paper and include the following:

- **KEY RESOURCES TABLE**
- **CONTACT FOR REAGENT AND RESOURCE SHARING**
- **EXPERIMENTAL MODEL AND SUBJECT DETAILS**
 - HCP dataset
 - Individual participant data
- **METHOD DETAILS**
 - HCP dataset
 - Individual participant data
- **QUANTIFICATION AND STATISTICAL ANALYSIS**
 - HCP dataset
 - Individual participants

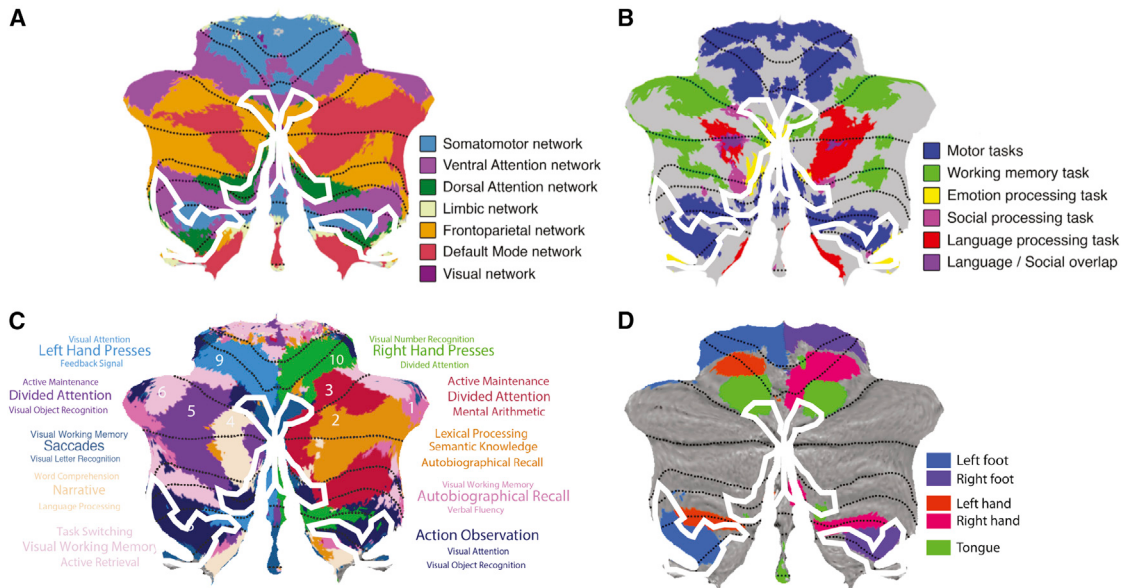


Figure 4. Location of Retinotopic Responses Relative to Known Cerebellar Topographies

Retinotopic maps from the current work are outlined in white.

- (A) Confirming previous findings [11, 13], our visual-spatial maps correspond primarily to visual and dorsal attention resting state networks and also include the somatomotor network in VIIIb [2].
- (B) Area VIIIb (and VIIb to a smaller extent) is activated by the HCP motor tasks [3].
- (C) Comparing to [5], OMV maps activate preferentially for saccades and visual working memory, and maps in VIIb and VIIIb correspond to regions involved in action observation and visual attention signaling.
- (D) Motor somatotopy maps from [18] show that region VIIIb overlaps best with foot-related regions.

● DATA AND SOFTWARE AVAILABILITY

- Code availability
- HCP retinotopy dataset
- Individual participant data

SUPPLEMENTAL INFORMATION

Supplemental Information can be found online at <https://doi.org/10.1016/j.cub.2019.04.012>.

ACKNOWLEDGMENTS

We would like to thank Serge Dumoulin and Jörn Diedrichsen for comments on previous versions of the manuscript. This research was made possible by grants from NWO (Middelgroot 480.12.009 to Spinoza Centre and NWO-CAS 012.200.012 awarded to T.K.).

AUTHOR CONTRIBUTIONS

Conceptualization, T.K.; Software, D.M.v.E.; Data Acquisition, D.M.v.E., T.K., and W.v.d.Z.; Formal Analysis, D.M.v.E.; Visualization, D.M.v.E.; Writing – Original Draft, D.M.v.E.; Writing – Review and Editing, D.M.v.E., T.K., and W.v.d.Z.

DECLARATION OF INTERESTS

The authors declare no competing interests.

Received: November 9, 2018

Revised: February 22, 2019

Accepted: April 4, 2019

Published: May 9, 2019

REFERENCES

1. Koziol, L.F., Budding, D., Andreasen, N., D'Arrigo, S., Bulgheroni, S., Imamizu, H., Ito, M., Manto, M., Marvel, C., Parker, K., et al. (2014). Consensus paper: the cerebellum's role in movement and cognition. *Cerebellum* 13, 151–177.
2. Buckner, R.L., Krienen, F.M., Castellanos, A., Diaz, J.C., and Yeo, B.T.T. (2011). The organization of the human cerebellum estimated by intrinsic functional connectivity. *J. Neurophysiol.* 106, 2322–2345.
3. Guell, X., Gabrieli, J.D.E., and Schmahmann, J.D. (2018). Triple representation of language, working memory, social and emotion processing in the cerebellum: convergent evidence from task and seed-based resting-state fMRI analyses in a single large cohort. *Neuroimage* 172, 437–449.
4. Stoodley, C.J., and Schmahmann, J.D. (2009). Functional topography in the human cerebellum: a meta-analysis of neuroimaging studies. *Neuroimage* 44, 489–501.
5. King, M., Hernandez-Castillo, C.R., Poldrack, R.A., Ivry, R.B., and Diedrichsen, J. (2019). A multi-domain task battery reveals functional boundaries in the human cerebellum. *bioRxiv*. <https://doi.org/10.1101/423509>.
6. Manni, E., and Petrosini, L. (2004). A century of cerebellar somatotopy: a debated representation. *Nat. Rev. Neurosci.* 5, 241–249.
7. Wandell, B.A., Dumoulin, S.O., and Brewer, A.A. (2007). Visual field maps in human cortex. *Neuron* 56, 366–383.
8. Swisher, J.D., Halko, M.A., Merabet, L.B., McMains, S.A., and Somers, D.C. (2007). Visual topography of human intraparietal sulcus. *J. Neurosci.* 27, 5326–5337.
9. Mackey, W.E., Winawer, J., and Curtis, C.E. (2017). Visual field map clusters in human frontoparietal cortex. *eLife* 6, e22974.
10. Chen, W., Zhu, X.H., Thulborn, K.R., and Ugurbil, K. (1999). Retinotopic mapping of lateral geniculate nucleus in humans using functional magnetic resonance imaging. *Proc. Natl. Acad. Sci. USA* 96, 2430–2434.

11. Brissenden, J.A., Levin, E.J., Osher, D.E., Halko, M.A., and Somers, D.C. (2016). Functional evidence for a cerebellar node of the dorsal attention network. *J. Neurosci.* 36, 6083–6096.
12. Marek, S., Siegel, J.S., Gordon, E.M., Raut, R.V., Gratton, C., Newbold, D.J., Ortega, M., Laumann, T.O., Adeyemo, B., Miller, D.B., et al. (2018). Spatial and temporal organization of the individual human cerebellum. *Neuron* 100, 977–993.e7.
13. Brissenden, J.A., Tobe, S.M., Osher, D.E., Levin, E.J., Halko, M.A., and Somers, D.C. (2018). Topographic cortico-cerebellar networks revealed by visual attention and working memory. *Curr. Biol.* 28, 3364–3372.e5.
14. Benson, N.C., Jamison, K.W., Arcaro, M.J., Vu, A., Glasser, M.F., Coalson, T.S., Van Essen, D.C., Yacoub, E., Ugurbil, K., Winawer, J., et al. (2018). The HCP 7T retinotopy dataset: description and pRF analysis. bioRxiv. <https://doi.org/10.1101/30824>.
15. Voogd, J., Schraa-Tam, C.K.L., van der Geest, J.N., and De Zeeuw, C.I. (2012). Visuomotor cerebellum in human and nonhuman primates. *Cerebellum* 11, 392–410.
16. Dumoulin, S.O., and Wandell, B.A. (2008). Population receptive field estimates in human visual cortex. *Neuroimage* 39, 647–660.
17. Pfaffenrot, V., Brunheim, S., Rietsch, S.H.G., Koopmans, P.J., Ernst, T.M., Kraff, O., Orzada, S., and Quick, H.H. (2018). An 8/15-channel Tx/Rx head neck RF coil combination with region-specific B_1 + shimming for whole-brain MRI focused on the cerebellum at 7T. *Magn. Reson. Med.* 80, 1252–1265.
18. Diedrichsen, J., and Zotow, E. (2015). Surface-based display of volume-averaged cerebellar imaging data. *PLoS ONE* 10, e0133402.
19. van Baarsen, K.M., Kleinnijenhuis, M., Jbabdi, S., Sotiroopoulos, S.N., Grotenhuis, J.A., and van Cappellen van Walsum, A.M. (2016). A probabilistic atlas of the cerebellar white matter. *Neuroimage* 124 (Pt A), 724–732.
20. Herzfeld, D.J., Kojima, Y., Soetedjo, R., and Shadmehr, R. (2015). Encoding of action by the Purkinje cells of the cerebellum. *Nature* 526, 439–442.
21. Thier, P., Dicke, P.W., Haas, R., and Barash, S. (2000). Encoding of movement time by populations of cerebellar Purkinje cells. *Nature* 405, 72–76.
22. Thomsen, K., Offenhauser, N., and Lauritzen, M. (2004). Principal neuron spiking: neither necessary nor sufficient for cerebral blood flow in rat cerebellum. *J. Physiol.* 560, 181–189.
23. Thomas, N.A., and Elias, L.J. (2011). Upper and lower visual field differences in perceptual asymmetries. *Brain Res.* 1387, 108–115.
24. Bressler, D.W., Fortenbaugh, F.C., Robertson, L.C., and Silver, M.A. (2013). Visual spatial attention enhances the amplitude of positive and negative fMRI responses to visual stimulation in an eccentricity-dependent manner. *Vision Res.* 85, 104–112.
25. van Es, D.M., Theeuwes, J., and Knapen, T. (2018). Spatial sampling in human visual cortex is modulated by both spatial and feature-based attention. *eLife* 7, 3771.
26. Van Essen, D.C. (2002). Surface-based atlases of cerebellar cortex in the human, macaque, and mouse. *Ann. N Y Acad. Sci.* 978, 468–479.
27. Kay, K.N., Winawer, J., Mezer, A., and Wandell, B.A. (2013). Compressive spatial summation in human visual cortex. *J. Neurophysiol.* 110, 481–494.

STAR★METHODS

KEY RESOURCES TABLE

REAGENT or RESOURCE	SOURCE	IDENTIFIER
Deposited Data		
HCP retinotopy dataset	online	https://balsa.wustl.edu/study/show/9Zkk .
Software and Algorithms		
Psychopy	online	https://www.psychopy.org/
Popeye	online	https://popeye.readthedocs.io/en/latest/popeye.html
FMRprep	online	https://github.com/poldracklab/fmriprep
Other		
7T MRI scanner	Philips	Achieva
8Tx/32Rx rf-coil	Nova Medical	N/A

CONTACT FOR REAGENT AND RESOURCE SHARING

Further information and requests for resources and reagents should be directed to and will be fulfilled by the Lead Contact, Dr. Tomas Knapen (tknapen@gmail.com).

EXPERIMENTAL MODEL AND SUBJECT DETAILS

HCP dataset

The pRF results presented in this manuscript are part of the 7T HCP retinotopy dataset. Please see the accompanying publication [14] for details on participants. Briefly, 181 participants participated in a 30 minute retinotopy experiment.

Individual participant data

In addition, three volunteers (two male, one female, age range 29-40) participated in a separate experiment after providing verbal and written informed consent. The medical ethical committee of the Amsterdam University Medical Centre, location VU, approved the experiments.

METHOD DETAILS

HCP dataset

The data collection and model fitting procedures are extensively described in [14]. Briefly, 181 participants performed a discrimination task at the fixation mark while viewing expanding and contracting rings, rotating wedges and traversing bar stimuli filled with fast-changing, random visual stimuli, for a total of approximately 30 minutes scan-time. The maximum eccentricity for these stimuli was 8 degrees of visual angle. Visual selectivity for each ‘gray-ordinate’ is modeled as a population receptive field (pRF) model. This is a uniform Gaussian distribution with free parameters of center (x and y), size (standard deviation), amplitude (with fixed sub-additive normalization constant of 0.05) and a baseline parameter. Functional MRI images were acquired at 7T using a spatial resolution of 1.6 mm, and in preprocessing interpolated to 2 mm isotropic. Individual runs were 5 minutes long and 300 time points each.

Individual participant data

The visual bar-shaped stimulus consisted of 2000 separate Gabor elements, each of which was assigned a random spatial frequency, orientation, colour and location within the bar. This bar traversed the entire screen in four directions (in temporal order: top-down (14 TRs), left-right (21 TRs), bottom-up (14 TRs), right-left (21 TRs)), stepping on every TR, with a 1 TR inter-bar interval. In top-bottom bar passes, bar width was 1/8th of screen height. For left-right bar passes, bar width was increased to assure equal area for horizontal and vertical bars, compensating for the aspect ratio of the 120 Hz, full HD (1920x1080) 32-inch BOLDScreen at the end of the bore. The screen extended 20 by 11 degrees of visual angle. Each TR was split into three epochs of 500ms. In the first and last epochs, the Gabors were grayscale. In the middle 500ms, the Gabors were randomly assigned one of two colour combinations (red/green or cyan/magenta). Participants had to indicate whether the majority of Gabor elements were red/green or blue/yellow. The ratio of Gabors that was assigned either colour combination was manipulated by a 3-up-1-down staircase procedure to ensure 79% correct separately for 4 different stimulus eccentricities. Attention to the bar ensures elevated BOLD responses [24], and this task

furthermore ensures equal attentional load regardless of stimulus location [25]. A white circular fixation circle at 0.15 degrees of visual angle in diameter was present at the centre of the screen at all times. Background colour was mid-grey.

Imaging data was acquired on a 7T system (Philips Achieva, NL) with an 8Tx/32Rx rf-coil for transmit and receive (Nova Medical Inc, USA). A 2-fold multiband accelerated 2D-EPI sequence was used for all functional imaging. The following set of parameters was used: FOV = 224*216*120 mm, resolution = 2*2*2 mm, TR = 1500 ms, TE = 22 ms, flip angle = 62 degrees, in-plane SENSE factor 2 (AP). Distortion correction was performed based on separately acquired opposite phase-encoding direction images, one for every pair of functional runs. The phases of the transmit channels were set to provide good signal homogeneity over the entire brain. Each run contained 120 volumes. The following numbers of runs were acquired per participant: S1: 37, S2: 47, S3: 36.

QUANTIFICATION AND STATISTICAL ANALYSIS

HCP dataset

Voxel selection procedure

To examine voxels that respond robustly to retinotopic stimuli, we first dismissed voxels where the pRF model explained little variance (see Figure S2, first column; thresholds determined in original paper [14] at 9.8% for the average and 2.2% for the individual participants). The threshold was determined by fitting a Gaussian Mixture Model with 2 Gaussians to the distribution of explained variances across voxels. The first distribution was assumed to be a noise pool, and the second a signal pool. The crossover point between the two Gaussians was then designated as the threshold that maximally separates noise from signal voxels. Second, the non-linear spatial transformations that were employed to align data across participants resulted in activity from ventral visual cortex to be smoothed into the cerebellar cortex. We were able to identify these voxels as these voxels were located between the cerebrum and cerebellum, and as these voxels were characterized by stark deviations in pRF parameter values (polar angle, eccentricity, size and explained variance; see areas indicated by white ovals in Figure S2). The resulting mask left many voxels with extremely low eccentricity and size, without clear polar angle progressions across voxels. We hypothesized the following as a generative mechanism for these voxels' results, following Benson et al. [14]. As participants performed a task on the fixation mark, this task became periodically more difficult when the retinotopic mapping stimulus passed behind the fixation mark. This means that responses of voxels sensitive to cognitive effort expended to maintain fixation (in a space-invariant manner) are in fact well captured by an extremely small and foveal pRF model. We therefore excluded voxels that extensively overlapped with the fixation point. As the fixation point extended to 0.15 dva eccentricity, we excluded voxels that had both a pRF eccentricity and size < 0.15 dva (see Figure S4, third column). This converts to a pRF - fixation point overlap of 26.7%–100%.

Cerebellar flatmaps

We used the SUIT toolbox [18] to project pRF results from three-dimensional volume space onto a flattened two-dimensional representation. Note that this flattened representation is compressed in the vertical dimension relative to a flattened representation that takes into account microscopic folding of individual cerebellum anatomy [26].

Participant ranking

In order to provide an estimate of the stability of the retinotopic maps in individual HCP participants (Figure S3), we ranked participants based on the median explained variance across voxels within the three retinotopic clusters determined in the average participant. In creating visualizations of polar angles in these participants, we masked voxels that fell outside the three retinotopic clusters as identified in the average participant and that were below the individual participant explained variance threshold of 2.2% (see 'Voxel selection procedure').

Individual participants

Following pre-processing by fMRIprep (<https://github.com/poldracklab/fmriprep>), data were spatially smoothed using a 3mm smoothing kernel. Slow drifts were removed using a savitzky-golay filter with a 120 s window. Then signals were converted to z-score on a per-run basis. Runs were subsequently averaged across runs weighted according to each runs' tSNR. A population receptive field model was fitted to the individuals' time courses on a voxel-by-voxel basis (<https://popeye.readthedocs.io/en/latest/popeye.html>) using a Compressive Spatial Summation (CSS) [27] model with parameters x, y, sigma en nonlinearity with 10-fold cross validation. Specifically, 10 different training sets were created by randomly selecting 75% of runs in each fold. Then, cross validated R2s were computed on the left out 25% of runs in each fold. A beta-mixture model was fitted on the resulting CV R2s across gray matter voxels to identify a 'signal' and 'noise' pool. Personalised R2 thresholds were taken such that a false-positive threshold of 0.01 was reached, (12/100 and 16/100 for participant 1 and 2, respectively). Subsequently, a non-specific 'bar-on' model was used to identify and exclude voxels which responded to any stimulus on the screen. Voxels where the pRF model variance explained exceeded the spatially unspecific model by more than 5% were entered into subsequent analyses.

DATA AND SOFTWARE AVAILABILITY

Code availability

The analysis code for creating the figures presented in this manuscript can be found under http://www.github.com/daanvanes/hcp_cerebellum_retinotopy. The atlas can be found on figshare under: 10.6084/m9.figshare.7751744, and finally the code to create

the individual participant maps and pRF experiment can be found under: https://github.com/daanvanes/cerebellum_prf. The raw data for the single-subject experiment are published on <https://openneuro.org/datasets/ds001851>.

HCP retinotopy dataset

The HCP retinotopy dataset can be sourced from: <https://balsa.wustl.edu/study/show/9Zkk>.

Individual participant data

The individual participant data are available on <https://openneuro.org/datasets/ds001851>.